Mercury isotopic compositions in fine particles and offshore surface seawater in a coastal area of East China: Implication for Hg sources and atmospheric transformations

Lingling Xu[a,b,*], Jiayan Shi[b,d], Yuping Chen[a,b,c], Yanru Zhang[a,b,c], Mengrong Yang[a,b], Yanting Chen[a,b], Liqian Yin[a,b], Lei Tong[a,b], Hang Xiao[a,b], Jinsheng Chen[a,b,*]

[a] *Center for Excellence in Regional Atmospheric Environment, Institute of Urban Environment, Chinese Academy of Sciences, Xiamen 361021, China*

[b] *Key Lab of Urban Environment and Health, Institute of Urban Environment, Chinese Academy of Sciences, Xiamen 361021, China*

[c] *University of Chinese Academy Sciences, Beijing 100049, China*

[d] *College of Resources and Environment, Fujian Agriculture and Forestry University, Fuzhou 350002, China*

* Corresponding author.

E-mail address: jschen@iue.ac.cn (J.S. Chen); linglingxu@iue.ac.cn (L.L. Xu)

Abstract. Isotopic compositions of Hg in atmospheric particles (Hg_{PM}) are probably the mixed results of emission sources and atmospheric processes. Here, we present Hg isotopic compositions in daily fine particles ($PM_{2.5}$) collected from an industrial site (CX) and a nearby mountain site (DMS) in a coastal area of East China, as well as in surface seawater close to the industrial area, to reveal the influence of anthropogenic emission sources and atmospheric transformations on Hg isotopes. The $PM_{2.5}$ samples displayed a significant spatial difference in δ^{202}Hg. For the CX, the negative δ^{202}Hg values are similar to those of source materials and the Hg_{PM} contents were well correlated with chemical tracers, indicating the dominant contributions of local industrial activities to $Hg_{PM2.5}$. Whereas the observed positive δ^{202}Hg at the DMS was likely associated with regional emissions and extended atmospheric processes during transport. The Δ^{199}Hg values in $PM_{2.5}$ from the CX and DMS were comparable positive. The unity slope of Δ^{199}Hg versus Δ^{201}Hg over all data suggests that the odd-MIF of $Hg_{PM2.5}$ was primarily induced by photo-reduction of Hg^{2+} in aerosols. The positive Δ^{200}Hg values with a minor spatial difference were probably associated with photo-oxidation of Hg^0 which is generally enhanced in the coastal environment. Total Hg in offshore surface seawater was characterized by negative δ^{202}Hg and near-zero Δ^{199}Hg and Δ^{200}Hg values, which are indistinguishable from Hg isotopes of source materials. Overall, the $PM_{2.5}$ collected from industrial areas had comparable δ^{202}Hg values but more positive Δ^{199}Hg and Δ^{200}Hg as compared to surface seawater. The results indicate that atmospheric transformations would induce significant fractionation of Hg isotopes and obscure the Hg isotopic signatures of anthropogenic emissions.

Keywords: Particle bound mercury; Surface seawater; Hg isotopes; Mercury sources; Photo-chemical processes.

1. Introduction

Mercury (Hg) is a genotoxic element and was ranked with the priority controlled pollutants in many countries. Atmospheric Hg was operationally defined as three forms: gaseous elemental mercury (GEM), gaseous oxidized mercury (GOM), and particle bound mercury (PBM or Hg_{PM}) (Schroeder and Munthe, 1998). Previous studies indicated that Hg_{PM} concentrations in urban and industrial areas could reach up to hundreds even thousands of pg m^{-3}, relative to tens of pg m^{-3} in uncontaminated remote areas (Fu et al., 2015; Mao et al., 2016). In addition, Hg_{PM} can account for up to 40% of atmospheric Hg in industrial areas, relative to < 5% in uncontaminated areas (Guo et al., 2022; Schroeder and Munthe, 1998). Hence, particulate matter (PM) can act as a vector of toxic Hg and inhalation of Hg-carrying particles is an important pathway of human exposure to atmospheric Hg. Coal combustion, non-ferrous metal smelting, and cement production were the three primary anthropogenic sources of atmospheric Hg, which are responsible for 47% of total global Hg emissions (GMA, 2018). On the other hand, Hg_{PM} undergoes complex transport and transformation processes in the atmosphere. Hg_{PM} can be formed by uptake of GOM in particles, which made an important contribution to Hg_{PM} in the heavily particle polluted areas (Xu et al., 2020). Whereas reduction of GOM binding with dissolved organic carbon ligands in aqueous particles potentially converts it back to the gas phase (Horowitz et al., 2017). In addition, Hg_{PM} has a residence time of several weeks as it can transport and deposit at a regional scale (Selin, 2009). The research has suggested that atmospheric Hg_{PM} is generally a combined result of anthropogenic emissions and atmospheric processes, which plays a crucial role in the global cycling of Hg.

Analysis technique of Hg isotopes and mechanisms of Hg isotopic fractionation have come a long way in the last decade (Blum and Johnson, 2017). Hg has seven stable isotopes (including ^{196}Hg, ^{198}Hg, ^{199}Hg, ^{200}Hg, ^{201}Hg, ^{202}Hg, and ^{204}Hg) and exhibits mass dependent fractionation (MDF) and mass independent fractionation (MIF) in various environmental samples and processes (Blum and Johnson, 2017; Sonke and Blum, 2013; Yin et al., 2014a). MDF of Hg isotopes is often reported as $\delta^{202}Hg$, while MIF of odd mass-numbered Hg isotopes (odd-MIF) is reported as

Δ^{199}Hg and Δ^{201}Hg and MIF of even Hg isotopes (even-MIF) as Δ^{200}Hg and Δ^{204}Hg. Previous laboratory and field studies have revealed that nearly all biogeochemical processes induce MDF of Hg isotopes, whereas significant odd-MIF of Hg occurs mainly in photochemical processes (Bergquist and Blum, 2007; Blum et al., 2014; Malinovsky et al., 2010; Sun et al., 2016a). What's more, specific ratios of Δ^{199}Hg/Δ^{201}Hg have been reported for different transformation processes, i.e., ~1.0 for photo-reduction of Hg^{2+} and ~1.6 for photo-oxidation of Hg^0 (Bergquist and Blum, 2007; Sun et al., 2016a). Even-MIF of Hg isotopes is observed mostly in atmosphere related samples, which is suggested to associate with photo-oxidation of Hg^0 by UV and oxidants (Blum and Johnson, 2017; Chen et al., 2012; Fu et al., 2019). Therefore, Hg isotopes are capable of becoming useful tracers for the biogeochemical cycles of Hg in the environment.

There is a large difficulty in sampling enough Hg mass for analyzing Hg isotopes of atmospheric samples. Even so, a few public studies have proved that Hg isotopes are useful tools to investigate potential sources and transformation processes of Hg in the atmosphere. The PM from major cities, like in northern and western China, mostly displayed significant negative MDF and near zero odd-MIF due to the dominant impact of anthropogenic emissions (Huang et al., 2015, 2016, 2019, 2020; Xu et al., 2017, 2019; Yu et al., 2016). A previous study conducted in remote areas of China has reported that the Hg_{PM} exposed to air masses of regional and long-range sources had distinct isotopic signatures (Fu et al., 2019). Recently, many studies have used Hg isotopes to investigate the contribution of domestic emissions and transboundary Hg transport to atmospheric Hg_{PM}. These studies have implied that the long-range transboundary Hg transport from South Asia played a crucial role in the Himalayas and the Tibetan Plateau, even in the southwestern and northwestern China (Fu et al., 2019; Guo et al., 2021, 2022). East China is densely populated and one of the heaviest industrialized area in China. The concentration of Hg_{PM} in this region has been well characterized (Hong et al., 2016; Xu et al., 2020; Yu et al., 2015), but only two studies conducted at the remote sites have referred to Hg_{PM} isotopes (Fu et al., 2019; Yu et al., 2016). To the best of our knowledge, there is no report on the isotopic compositions of

Hg_{PM} from urban areas of East China. Likewise, the effect of atmospheric processes on the fractionation of Hg isotopes in the coastal region has not been well elucidated.

This study determined Hg isotopic compositions in $PM_{2.5}$ collected from an industrial site and a mountain site in a coastal area of East China. Comparison of $Hg_{PM2.5}$ isotopes at the neighboring sites would eliminate the impacts of meteorology and atmospheric Hg background which vary across space on Hg_{PM} isotopes. Furthermore, this study measured the isotopic compositions of total mercury (THg) in surface seawater close to the industrial area and distinguished Hg isotopes between the atmospheric sample and surface medias. The objectives of this study are (1) to differentiate the Hg isotopes in $PM_{2.5}$ from the two neighboring industrial and mountain sites; (2) use the Hg isotopes to explore the influence of anthropogenic sources on the Hg_{PM}; (3) to reveal the role of atmospheric transformations in varying Hg_{PM} isotopic compositions.

2. Experiment

2.1. Study area description

$PM_{2.5}$ sampling was conducted at an industrial site (Chunxiao, CX) and a nearby mountain site (Daimeishan, DMS) on the east coast of Zhejiang province, East China (Fig. 1). The study region experiences a typical subtropical monsoon climate, with sea breeze in summer and continental breeze in winter. The average annual temperature, precipitation, relative humidity, and sunshine hours were 18.1 ℃, 1608 mm, 76.8%, and 1797 h, respectively.

The CX (121.91 °E, 29.87 °N, 15 m a.g.l.) is located in the Urban Environment Observation and Research Station, Chinese Academy of Sciences, Beilun District, Ningbo. Ningbo is a highly industrial city and there is a high density of industrial activities around the CX. Potential Hg point sources include a large coal-fired power plant (5000 MW) approximately 20 km to the northwest, a Chlor-alkali plant 20 km to the northeast, and an automobile assembly plant within 1 km of the site. The CX is in close proximity to the East China Sea (ECS, ~ 0.6 km), thus clean air masses from the sea in warm seasons would dilute atmospheric Hg at the CX.

The DMS (121.62 ° E, 29.68 ° N, 450 m a.s.l.) is located at the summit of

Mountain Damei, which is surrounded by trees. The site is 20 km to the coast of the ECS and approximately 22 km south of Ningbo. There are no significant Hg point sources within a radius of ~10 km from the DMS. However, an early study reported that intense regional emissions, like industrial activities and coal combustion in the Yangtze River Delta and the neighboring region of Anhui, Jiangsu, and Zhejiang Provinces, caused a high atmospheric Hg concentration at the DMS (Yu et al., 2015).

Surface seawater samples were collected in the offshore area of Ningbo. The seawater sampling area (about 122.04 ° E, 29.82 ° N, Fig. 1) is approximately 1 km west of the Beilun District, Ningbo. The salinity of the seawater samples ranged from 21.2‰ to 29.5‰. The pH of the seawater samples was in the range of 5.7 ~ 8.5, with the mean value of 7.5 ± 0.6.

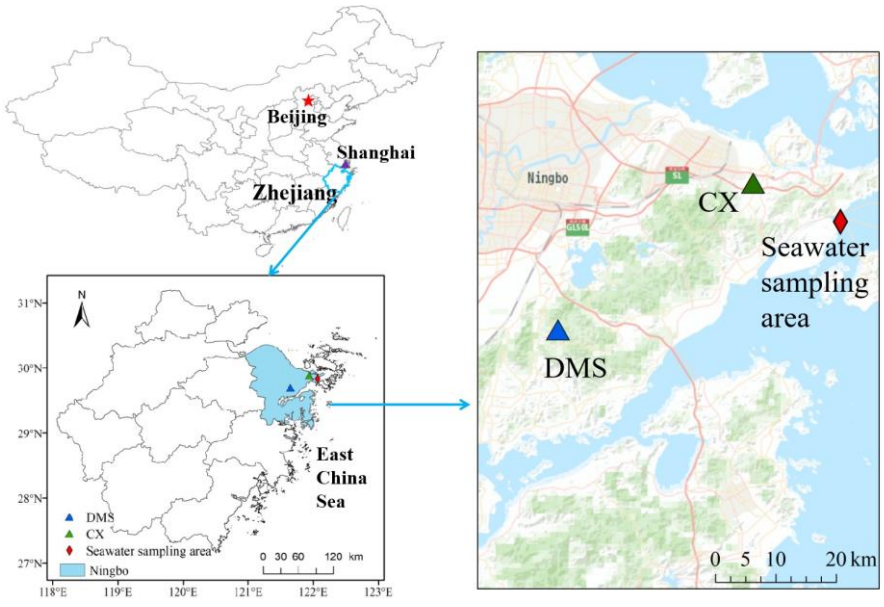

Fig. 1 Locations of $PM_{2.5}$ (CX: industrial site; DMS: mountain site) and surface seawater sampling area.

2.2. Sample collection and analysis

2.2.1. Sampling of $PM_{2.5}$

The period of $PM_{2.5}$ sampling was from Jul. 2017 to Jun. 2018. Daily $PM_{2.5}$ samples were collected 1~2 times a week at the CX (except Jan. and Feb. 2018) and once a week at the DMS. Field blank samples were collected at each site. $PM_{2.5}$ samples were collected on a preheated quartz-fiber filter (500 ℃, 4 h, 8 × 10 inches, Whatman) using a high volume sampler (Tianhong TH1000H, China) with a flow rate

of 1.05 m^3 min^{-1}. The filters were conditioned at 24 ± 1 °C and 52 ± 2%. The mass loading of $PM_{2.5}$ on filters was determined by mass difference before and after sampling. The filter samples were wrapped in aluminum foils and stored at -20 °C until analysis.

2.2.2. Concentration of Hg and other chemical species in $PM_{2.5}$

Six punches (ca. 0.5 cm^2 per punch) of each sampling filter were digested by a 10 mL of 40% aqua regia (HNO_3: HCl = 1:3, *v/v*) in a water bath at 95 °C for 5 min, then the solution was oxidized by 1 mL of 0.2 M BrCl and bathed for another 30 min. After cooling down, the extracted solution was diluted to 15 mL with ultra-pure water and then analyzed by cold-vapor atomic fluorescence spectrometry (CVAFS, Brooks Rand Model III, USA) following the EPA method 1631. The content of Hg on blank filters can be negligible (42.5 pg at the CX and 27.0 pg at the DMS) relative to those on sample filters.

$PM_{2.5}$ samples selected for Hg isotopes analysis were also measured for 8 water soluble inorganic ions (K^+, Ca^{2+}, Na^+, Mg^{2+}, Cl^-, SO_4^{2-}, NO_3^-, and NH_4^+), elemental carbon (EC), organic carbon (OC), and levoglucosan. The water soluble ions were analyzed by ion chromatography (ICS-3000, Dionex, USA). EC and OC were analyzed using a carbon analyzer (Model 4, Sunset Lab., USA) and NOISH protocol. Analytical procedures and quality control procedures have been described by Xu et al. (2018). Levoglucosan, an excellent indicator of biomass burning, was analyzed using a gas chromatography – mass spectrometer detector (GC – MS, Agilent 7890A-5975C, Agilent Tech. Inc., USA). Levoglucosan analytical procedures have been presented in detail elsewhere (Hong et al., 2019).

2.2.3. Sampling and analysis of Hg in seawater

Seawater samples were collected from the surface of the offshore sampling area twice a month during Jul. 2017 ~ Jun. 2018, except Feb. 2018. Each time, three ~50 mL of duplicate seawater samples were collected for THg content analysis. Final THg content was determined by the average of three duplicate samples. In addition, ~2 L surface seawater was sampled for Hg isotopes analysis each time. The seawater samples were stored in brown glass bottles and preserved with 1% (*v/v*) HCl in the

laboratory. They were analyzed for Hg content and isotopic compositions in a month.

Total Hg content in seawater samples was measured by CVAFS (Brooks Rand Model III, USA). A 25 mL of seawater sample was digested with 0.2 M BrCl at least 12 h in advance and then analyzed using the EPA method 1631. More details can be found in a previous study (Xu et al., 2014). Method blank was processed by bottles filling up with ultra-pure water instead of seawater. The blank was lower than 10 pg (n = 15), which can be negligible compared to the samples.

2.3. Analysis of Hg isotopic compositions

2.3.1. $PM_{2.5}$ sample processing

Due to the effects of precipitation and short sampling duration, the mass of Hg on most of $PM_{2.5}$ samples was not sufficient for isotopes detection. A total of 20 $PM_{2.5}$ samples, including 10 at the CX and 10 at the DMS, were chosen for Hg isotopes analysis. Pre-concentration of Hg from $PM_{2.5}$ samples was conducted following a dual-stage combustion protocol (Huang et al., 2015). To be specific, a tube furnace (OTF-1200X-Π, Kejin, China) consisting of two combustion stages was used. A sampling filter was embedded in a furnace quartz tube (50 mm OD, 46 mm ID, 80 cm length). The tube was then placed in the furnace so that the filter was at the first combustion stage. The second decomposition stage was heated up in advance and maintained at 1000 ^{o}C, then the first combustion stage was heated up to 950 ^{o}C through a temperature-programmed procedure. The combustion procedure was run with no samples in the furnace quartz tube before $PM_{2.5}$ sample treatment every day to remove residual volatiles. The released Hg was transferred by O_2/Ar gas (30%/70%) at a flow rate of 20 mL min^{-1} and then trapped by a 10 mL of 40% inverse aqua regia (2: 4: 9 ratio of 10 M HCl, 15 M HNO_3 and ultra-pure water) in a designed glass bottle. In advance of $PM_{2.5}$ sample analysis, the accuracy of dual-stage combustion method was assessed by the analysis of the standard NIST SRM 3133 Hg (dripped on blank filters) and the certified reference material GBW07434. The Hg recovery efficiency of the dual-stage protocol was in the range of 87.6% ~ 103.3% (mean: 95.0 ± 5.1%, n = 6).

2.3.2. Seawater sample processing

A total of 20 seawater samples were analyzed for Hg isotopes. ~2 L seawater sample was mixed with a 4 mL of 300 g L^{-1} NH_2OH·HCl solution for neutralizing excess BrCl and then an 8 mL of 200 g L^{-1} $SnCl_2$ solution for reducing the oxidized Hg. The pre-treated seawater sample was stirred and bubbled for 1 h with Hg-free N_2 at a flow rate of 400 mL min^{-1}. The gaseous Hg purged off seawater samples was collected by a series of three gold traps. The gold traps were heated and the released Hg was transferred by Hg-free N_2 at 10~15 mL min^{-1} and concentrated by a 10 mL of 40% inverse aqua regia.

2.3.3. Hg isotopes analysis

All trapping solutions were preserved with 1% (*v/v*) BrCl and stored at 4 °C in the dark before Hg isotopes analysis. Hg isotopic compositions were measured by a multi–collector inductively coupled plasma mass spectrometer (MC-ICP-MS, Nu Instruments Ltd. UK) equipped with an introduction device following the protocols presented in previous studies (Huang et al., 2015; Huang et al., 2021; Lin et al., 2015). The introduction device includes a modified cold-vapor generator (CVG) and an Aridus III nebulizer for respective Hg and Tl introduction. Between standard and sample, the CVG was rinsed with 3% (v/v) HNO_3 solution to ensure the Hg signal returned to the background level. Instrument mass bias was corrected using both an internal standard (NIST 997 Tl) and a strict sample-standard bracketing method (NIST 3133 Hg). A reference material NIST 8610 was measured repeatedly for quality control. The pre-concentration solutions were diluted to about 1.5 ~ 3.0 ng mL^{-1} and the NIST 3133 and NIST 8610 were kept at 2.0 ng mL^{-1} during the analysis period. The MDF of Hg (represented by δ-value, ‰) is defined by the following equation (Blum and Bergquist, 2007):

$$\delta^{xxx}Hg\ (‰) = [(^{xxx}Hg/^{198}Hg)_{sample}/(^{xxx}Hg/^{198}Hg)_{NIST\ 3133} - 1] \times 1000 \quad (1)$$

where xxx = 199, 200, 201, and 202. The MIF of Hg (Δ-value, ‰) is calculated using the theoretically predicted MDF as the following equation (Blum and Bergquist, 2007):

$$\Delta^{xxx}Hg\ (‰) = \delta^{xxx}Hg - (\delta^{202}Hg \times \beta) \quad (2)$$

where the mass-dependent scaling factor β is 0.252 for ^{199}Hg, 0.502 for ^{200}Hg, and

0.752 for ^{201}Hg. The repeated measurement of NIST 8610 during the analysis session yielded δ^{202}Hg and Δ^{199}Hg values of -0.60 ± 0.15‰ and -0.02 ± 0.06‰ (2σ, n = 7). In addition, a well-known reference material UM-Almaden showed a long-term average of δ^{202}Hg = -0.59 ± 0.10‰ and Δ^{199}Hg = -0.03 ± 0.07‰ (2σ, n = 25), which are well consistent with those in previous studies (Blum and Bergquist, 2007; Huang et al., 2015). The samples of this study were measured only once, so the 2σ uncertainties derived from repeated measurements of NIST 3133 standard during each analysis section were applied to the samples.

3. Results and discussion

3.1. Concentrations and isotopic compositions of $Hg_{PM2.5}$

Concentrations and isotopes of $Hg_{PM2.5}$ at industrial and mountain sites are showed in Table 1. Mean volumetric concentrations of $Hg_{PM2.5}$ were 16.3 ± 17.8 pg m^{-3} at the CX and 29.6 ± 35.9 pg m^{-3} at the DMS, which are comparable to those observed at remote sites (Fu et al., 2019), but lower than those reported from urban sites in China (Xu et al., 2019). The low volumetric concentrations of $Hg_{PM2.5}$ observed in this study were likely associated with low $PM_{2.5}$ concentrations (mean: 28.0 μg m^{-3} at the CX and 34.8 μg m^{-3} at the DMS) during the study period. Average mass concentrations of $Hg_{PM2.5}$ were 0.52 ± 0.23 μg g^{-1} (0.15 to 1.10, n = 51) at the CX and 0.85 ± 0.63 μg g^{-1} (0.18 to 2.80, n = 33) at the DMS, respectively. A relatively high concentration of $Hg_{PM2.5}$ has been reported at the DMS before, which was likely due to regional Hg emissions, mainly the industrial activities and coal combustion in the Yangtze River Delta and the neighboring region of Anhui, Jiangsu, and Zhejiang Provinces (Yu et al., 2015). The Hg contents in $PM_{2.5}$ of this study are higher than those of natural sources (e.g., dust and topsoil; 0.056 ~ 0.30 μg g^{-1}; Schleicher et al., 2015) and those of coals in China (mean: 0.22 μg g^{-1}; Yin et al., 2014b), which implies a potential contribution of anthropogenic sources with high Hg contents. The volumetric concentrations of $Hg_{PM2.5}$ were closely correlated to $Hg_{PM2.5}/PM_{2.5}$ ratios both at the CX and DMS (R^2 = 0.50 and 0.60, p < 0.01), suggesting that atmospheric $Hg_{PM2.5}$ concentrations were dependent on Hg contents. Whereas, a weak correlation between the $Hg_{PM2.5}$ volumetric concentrations and $PM_{2.5}$

masses was observed at the DMS (R^2 = 0.25, p < 0.01) in contrast to the CX (R^2 = 0.77, p < 0.01). The result likely indicates that the DMS $Hg_{PM2.5}$ was influenced by diverse sources of $PM_{2.5}$ with different Hg levels and/or complex atmospheric Hg transformations (Xu et al., 2019). This is supported by the higher variation coefficient (VC = SD/Mean) of $Hg_{PM2.5}$ mass concentrations at the DMS (74.1%) than the CX (44.2%). Spatial differences of $Hg_{PM2.5}$ were further examined by relationships of Hg with other chemical species in $PM_{2.5}$ (Table S1). In contrast to DMS, the mass concentrations of $Hg_{PM2.5}$ at the CX were well correlated to chemical tracers, like Cl^-, NO_3^-, K^+, and OC (r = 0.40 ~ 0.57, p < 0.05, Spearman correlation), implying the contributions of steady anthropogenic sources to $Hg_{PM2.5}$ in the industrial area.

δ^{202}Hg values for $Hg_{PM2.5}$ at the CX were in the range of -1.11‰ to 0.08‰ (mean: -0.61 ±0.35‰, n = 10), while δ^{202}Hg values at the DMS were significantly higher and in a larger variation from -0.78‰ to 1.10‰ (mean: 0.12 ±0.63‰, n = 10) (p < 0.05, T Test; Table 1 and Table S2). Hg_{PM} isotopic compositions in multiple types of locations are showed in Fig. 2 and Table S3. The δ^{202}Hg values at the CX basically overlap those for PM in urban areas of China (mean: from -1.60‰ to -0.42‰), as well as those for major source materials such as coal combustion, smelting, and cement plants (mean: -1.10‰, -0.87‰, and -1.42‰ respectively, Huang et al., 2016) and those for PM near anthropogenic emissions such as industry, landfill, traffic, and coal-fired power plants (mean: from -2.41‰ to -0.58‰) (Fig. 2). The result likely indicates an important contribution of anthropogenic sources to the CX $Hg_{PM2.5}$. However, the δ^{202}Hg values of above mentioned potential sources are not distinguishable, thus we could not identify the specific sources of $Hg_{PM2.5}$ solely based on Hg isotopes. On the other hand, the slight positive δ^{202}Hg values at the DMS are quite different from those observed at remote sites (mean: from -1.45‰ to -0.83‰; Fig. 2). Nevertheless, a less negative MDF of $Hg_{PM2.5}$ has also been reported at the DMS in a previous study (δ^{202}Hg = -0.26‰, Yu et al., 2016). Hg_{PM} from immediate anthropogenic emissions is generally characterized by negative δ^{202}Hg, which in turn suggests that the more positive δ^{202}Hg of Hg_{PM} at the DMS might be affected by atmospheric processes, like photo-reduction of Hg^{2+} (Bergquist and Blum, 2007; Zheng and Hintelmann, 2009).

In contrast to MDF, the odd-MIF of $Hg_{PM2.5}$ at the two sites were comparable ($p > 0.05$, *T* Test), with $\Delta^{199}Hg$ values of 0.17 ± 0.22‰ (from -0.17‰ to 0.52‰) at the CX and 0.16 ± 0.24‰ (from -0.22‰ to 0.47‰) at the DMS, respectively. The significant positive $\Delta^{199}Hg$ in this study are similar to those observed in coastal areas (Rolison et al., 2013; Yu et al., 2020) and in remote areas in China (Fu et al., 2019), but distinguishable from those in urban and industrial areas with near-zero values due to anthropogenic emissions (Das et al., 2016; Huang et al., 2016, 2018, 2020; Xu et al., 2019; Yu et al., 2016). A laboratory study has indicated that photo-reduction of Hg^{2+} restrains odd Hg in reactants (aerosols here) in priority, which shifts $\Delta^{199}Hg$ values positively (Bergquist and Blum, 2007). Thus, it's reasonably supposed that the positive odd-MIF of Hg_{PM} in the study region was associated with photo-reduction of Hg^{2+} in aerosols. As shown in Table S2 and Fig. S1, $PM_{2.5}$ samples affected by long range transport of air masses mostly had large positive $\Delta^{199}Hg$, like $PM_{2.5}$ collected on Apr. 4, 2018 from the CX and on Jan. 10, 2018 from the DMS. It's probably related to extensive photo-reduction of Hg^{2+} in aerosols during long-range transport, as previous studies suggested (Fu et al., 2019; Huang et al., 2016). In addition, the MIF of ^{200}Hg, most probably relating to photo-reactions, was significant positive and displayed no spatial difference (0.11 ± 0.07‰ at the CX and 0.14 ± 0.07‰ at the DMS; $p > 0.05$, *T* Test), which suggests enhanced and homogeneous photo-reactions in the study region. It is worth noting that a part of $PM_{2.5}$ samples collected from the DMS displayed negative $\delta^{202}Hg$ and near-zero $\Delta^{199}Hg$, similar to those from the CX (Fig. 2). Compared with the previous study (Yu et al., 2016), our results provide isotopes evidence that $Hg_{PM2.5}$ at the DMS was affected by multiple sources and one of them might be regional anthropogenic emissions.

Table 1 Concentrations and isotopic compositions of $Hg_{PM2.5}$ at the industrial site (CX) and mountain site (DMS) in East China

Parameter [a]	CX		DMS	
	Mean ± sd	Range	Mean ± sd	Range
$Hg_{PM2.5}$ (μg g^{-1})	0.52 ± 0.23	0.15 ~ 1.10	0.85 ± 0.63	0.18 ~ 2.80
$Hg_{PM2.5}$ (pg m^{-3})	16.3 ± 17.8	1.6 ~ 90.7	29.6 ± 35.9	2.9 ~ 181.3
$PM_{2.5}$ (μg m^{-3})	28.0 ± 19.8	1.6 ~ 82.2	34.8 ± 20.3	3.4 ~ 72.2

δ^{202}Hg (‰)	-0.61 ± 0.35	-1.11 ~ 0.08	0.12 ± 0.63	-0.78 ~ 1.10
Δ^{199}Hg (‰)	0.17 ± 0.22	-0.17 ~ 0.52	0.16 ± 0.24	-0.22 ~ 0.47
Δ^{201}Hg (‰)	0.21 ± 0.18	-0.07 ~ 0.48	0.23 ± 0.36	-0.29 ~ 0.66
Δ^{200}Hg (‰)	0.11 ± 0.07	-0.01 ~ 0.23	0.14 ± 0.07	0.06 ~ 0.28
Δ^{204}Hg (‰)	0.19 ± 0.36	-0.16 ~ 0.93	3.58 ± 3.68	0.26 ~ 11.38

[a] 51 samples collected from CX and 32 samples from DMS were used for $Hg_{PM2.5}$ concentration analysis; 10 samples from each site for isotope analysis.

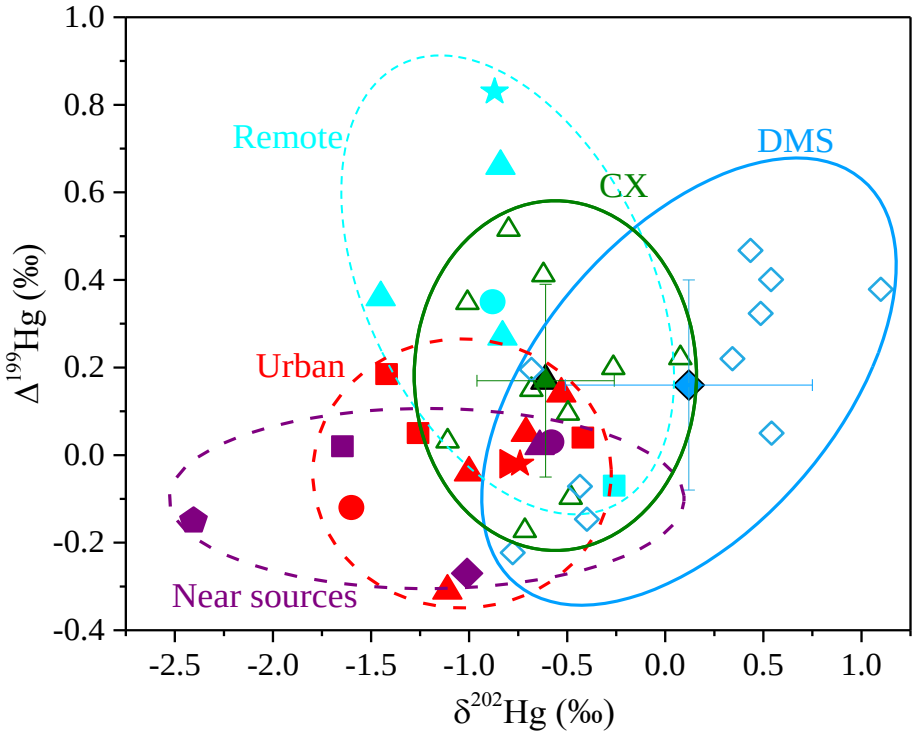

Fig. 2 Isotopic compositions of Hg_{PM} at the multiple types of sites (This study: ▲△mean and each values at the CX, ◆◇mean and each values at the DMS; Remote sites: ★coast, ■▲mountain, ●island (Fu et al., 2019; Rolison et al., 2013; Yu et al., 2016); Urban sites in China: ▲Beijing, ●Changchun, ★Chengdu, ■Guiyang, ▶Xi'an (Huang et al., 2015, 2016, 2019, 2020; Xu et al., 2017, 2019; Yu et al., 2016); Sites near emission sources: ▲■industrial, ⬟landfill, ◆traffic, ★near CFPP (Das et al., 2016; Huang et al., 2018; Yu et al., 2016)

3.2. Influence of anthropogenic emissions on MDF of $Hg_{PM2.5}$

Prior studies have compiled Hg isotopic compositions of major source materials, such as fossil fuels, non-ferrous metal ores, and crustal rocks, which generally display large negative δ^{202}Hg and negative or near-zero Δ^{199}Hg values (Huang et al., 2016; Sun et al., 2016b). Combustion or/and industrial processing induces limited MIF (Sun et al., 2013; Sun et al., 2016b), so we assumed that emitted Hg conserves the odd isotope MIF of source materials. The Δ^{199}Hg values for most of the $Hg_{PM2.5}$ samples are distinguishable from those of source materials, indicating that anthropogenic

emissions were not the drive factors for odd-MIF of $Hg_{PM2.5}$ in the study region. As for MDF, the above analyses indicated that the MDF of $Hg_{PM2.5}$ at the CX was subjected to local anthropogenic sources, while the MDF at the DMS was probably caused by the combination of atmospheric transformations and regional emissions. The result was supported by the correlation between $\delta^{202}Hg$ values and $Hg_{PM2.5}$ concentrations which was insignificant at the DMS, but significant at a loose level at the CX (Fig. 3a). Pearson correlation between $\delta^{202}Hg$ and chemical components was further conducted to explore the impacts of anthropogenic emissions on $Hg_{PM2.5}$.

The $\delta^{202}Hg$ values at the CX were significantly correlated to Cl^- content (R^2 = 0.46, $P < 0.05$, Fig. 3b) and well associated with SO_4^{2-} content in $PM_{2.5}$ (R^2 = 0.38, P = 0.056, Fig. 3c). In this study, Cl^- was mainly originated from coal combustion, given that Cl^- content in $PM_{2.5}$ was not correlated to Na^+. Besides, SO_4^{2-} was primarily transformed from SO_2 which is mainly emitted from coal combustion. The results imply that coal combustion played an important role in the MDF of $Hg_{PM2.5}$ at the CX. It has also been reported that coal combustion has a large contribution of ~50% to total Hg emissions in Zhejiang province (Zhang et al., 2015). Differently from the CX, the $\delta^{202}Hg$ values at the DMS were significantly correlated to SO_4^{2-} (R^2 = 0.68, $P < 0.05$, Fig. 3c), but not to Cl^- ($P > 0.05$, Table S4). It seems unlikely that coal combustion was the predominant contributor to the positive MDF at the DMS. Whereas under the influence of transport, the transformation of SO_2 to SO_4^{2-} usually enhances and the photo-reduction of Hg^{2+} in aerosols tends to extensive which would shift $\delta^{202}Hg$ to positive to a certain extent (Bergquist and Blum, 2007). The results imply that coal combustion emissions at a regional scale or from long--range transport had a potential impact on the MDF of $Hg_{PM2.5}$ at the DMS, which is consistent with an earlier study conducted at the same site based on Hg concentration and trajectory analysis (Yu et al., 2015).

It should be noted that the $\delta^{202}Hg$ values at the CX slightly shift to positive compared to those for emitted Hg_{PM} from coal combustion. Hg isotopic compositions of coals in China have large variations in MDF with $\delta^{202}Hg$ values from -2.36‰ to -0.14‰ (Biswas et al., 2008; Yin et al., 2014b). A prior study estimated that emitted

Hg_{PM} has a shift of -0.5‰ relative to $\delta^{202}Hg$ of coal feeds based on the mass balance model (Sun et al., 2014). Then $\delta^{202}Hg$ values for Hg_{PM} emitted from coal combustion in China were estimated to be -2.86‰ to -0.64‰. There are many metal smelting factories near the CX. Although we did not measure the tracers for smelting, the mean $\delta^{202}Hg$ value for non-ferrous metal ores was reported to be -0.47 ± 0.77‰ (Yin et al., 2016). We assumed that Hg emitted from non-ferrous metal smelting conserves the isotopes of source materials due to a lack of data for processing at the current stage (Sun et al., 2016b). Then, less negative MDF of Hg from non-ferrous metal smelting could explain the positive-shift MDF at the CX relative to coal combustion emissions. Thus, it is reasonably inferred that the MDF of $Hg_{PM2.5}$ at the CX is a result of multiple anthropogenic sources such as coal combustion and non-ferrous metal smelting.

In addition, we found a close negative correlation between $\delta^{202}Hg$ and levoglucosan content in $PM_{2.5}$ at the CX (R^2 = 0.67, P < 0.05, Fig. 3d) excluding a $PM_{2.5}$ sample collected on Dec. 19, 2017. Levoglucosan is considered an excellent indicative of biomass burning. Thus, we cannot rule out the possibility that the contribution of biomass burning led to a negative deviation of $\delta^{202}Hg$ values at the CX to some extent. Previous studies have reported that biological materials display negative $\delta^{202}Hg$ and $\Delta^{199}Hg$ values, like foliage ($\delta^{202}Hg$: -2.67‰ to -1.79‰; $\Delta^{199}Hg$: -0.47‰ to -0.06‰), litterfall samples ($\delta^{202}Hg$: -3.03‰ to -2.35‰; $\Delta^{199}Hg$: -0.44‰ to -0.22‰), and lichen ($\delta^{202}Hg$: -2.32‰ to -1.83‰; $\Delta^{199}Hg$: -0.35‰ to -0.22‰) (Demers et al., 2013; Jiskra et al., 2015; Yin et al., 2013; Yu et al., 2016; Zheng et al., 2016). Such negative $\delta^{202}Hg$ and $\Delta^{199}Hg$ of biological materials could not explain the isotopes of $Hg_{PM2.5}$ in this study. Moreover, the contribution of biomass burning is supposed to shift $\Delta^{199}Hg$ values negatively, but we found no significant negative correlation between $\Delta^{199}Hg$ and K^+ or levoglucosan from the whole study period (Table S4). This unexpected result might be due to the fact that the substantial biomass burning often occurs in a short time (i.e., Mar. 2018, Fig. S2a, *https://firms.modaps.eosdis.nasa.gov/*). In this study, the most negative odd-MIF was observed for $PM_{2.5}$ samples collected on Mar. 21, 2018, with a $\Delta^{199}Hg$ value of

-0.17‰ at the CX and -0.22‰ at the DMS. Those $PM_{2.5}$ samples were likely related to biomass burning, since they were associated with air masses originating from or passing through the northeast of China with dense fire spots (Fig. S2b). The findings suggest the biomass burning was not the dominant contributor of $Hg_{PM2.5}$ in the study region, but it would change the isotopes of $Hg_{PM2.5}$ in some times.

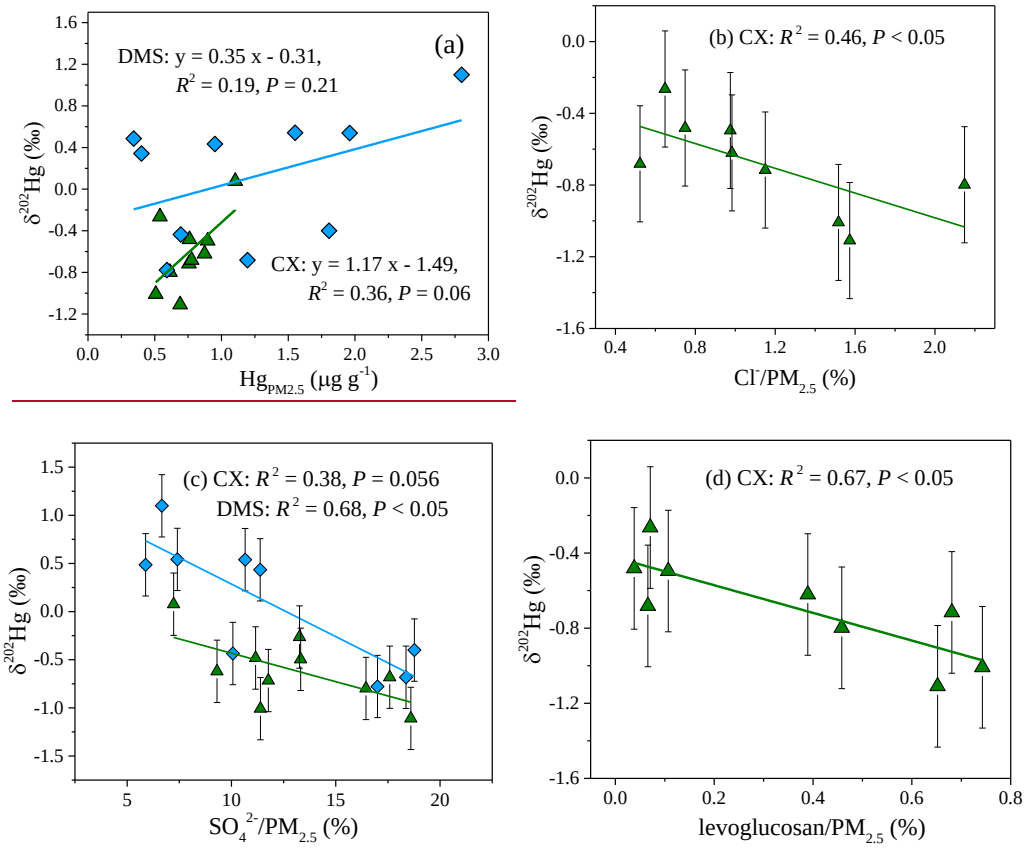

Fig. 3 Relationships of $\delta^{202}Hg$ with (a)Hg, (b) Cl^-, (c) SO_4^{2-}, and (d) levoglucosan contents in $PM_{2.5}$ at CX (▲) or DMS (◆). Uncertainty (2σ) for $\delta^{202}Hg$ in $PM_{2.5}$ is 0.25‰.

3.3. Influence of photo-chemical processes on isotopes of $Hg_{PM2.5}$

Large odd-MIF of Hg isotopes in most $PM_{2.5}$ samples of this study was likely related to photo-chemical processes. An experiment study has found that the oxidation of Hg^0 by halogen atoms (Cl· or Br·) results in a negative shift of $\Delta^{199}Hg$ in product Hg^{2+} (Sun et al., 2016a). Given that partitioning of Hg^{2+} between gas and particle phases leads to limited odd-MIF of Hg isotopes (Fu et al., 2019; Wiederhold et al., 2010), the formation of Hg_{PM} via oxidation of Hg^0 and following adsorption on particles could not explain the positive odd-MIF of $Hg_{PM2.5}$ in this study. Previous experiments and field studies have reported that photo-reduction of inorganic Hg^{2+} in

the aqueous solution induces odd-MIF of Hg isotopes and results in large positive Δ^{199}Hg values in reactants (aerosols here, Bergquist and Blum, 2007; Zheng and Hintelmann, 2009). Hence, photo-reduction of Hg^{2+} in aerosols was invoked as a key factor for the odd-MIF of $Hg_{PM2.5}$ in the study region. The linear relationship between Δ^{199}Hg and Δ^{201}Hg is often used to identify the odd-MIF processes of Hg isotopes. The slope of Δ^{199}Hg versus Δ^{201}Hg yielded from the data of each site was 1.16 (R^2 = 0.92) at the CX and 0.63 (R^2 = 0.85) at the DMS, respectively. The data over the two sites defined a straight line with a slope of 0.92 (R^2 = 0.83, P < 0.01; Fig. 4a). The near-unity slope of Δ^{199}Hg versus Δ^{201}Hg was widely observed in particles from coastal site and from other locations in Asia (Fu et al., 2019; Rolison et al., 2013; Huang et al., 2016, 2019; Xu et al., 2019). The Δ^{199}Hg/Δ^{201}Hg ratios of this study are more consistent with the indicative ratio of aqueous photo-reduction of inorganic Hg^{2+} (~1.0, Bergquist and Blum, 2007; Zheng and Hintelmann, 2009), but different from the ratios of other processes, like photo-oxidation (1.64 by Br· and 1.89 by Cl·, Sun et al., 2016) and photo-demethylation (1.36, Bergquist and Blum, 2007). Therefore, the photo-reduction of Hg^{2+} in aerosols might be the critical factor for the observed positive odd-MIF of $Hg_{PM2.5}$ in the study region.

The similarity of odd-MIF anomaly between the CX and DMS suggests the photo-reduction of Hg^{2+} in aerosols was homogeneous at a regional scale. However, the relationships of Δ^{199}Hg with $Hg_{PM2.5}$ content and δ^{202}Hg showed distinct spatial differences. For the DMS, the Δ^{199}Hg values generally decreased with $Hg_{PM2.5}$ content increased (Fig. 4b) and the correlation between Δ^{199}Hg and δ^{202}Hg was significantly positive (R^2 = 0.56, P < 0.05; Fig. 4c). Experimental studies indicated that photo-reduction of Hg^{2+} releases Hg^0 and preferentially retains odd and heavier isotopes in solutions (Bergquist and Blum, 2007; Zheng and Hintelmann, 2009), which is expected to result in a positive relationship between Δ^{199}Hg and δ^{202}Hg and an inverse relationship between Δ^{199}Hg and $Hg_{PM2.5}$ content. In this study, the consistent relationships of Δ^{199}Hg with δ^{202}Hg and $Hg_{PM2.5}$ at the DMS strongly imply a predominant role of photo-reduction of Hg^{2+} in isotopic fractionation of $Hg_{PM2.5}$ at this site. Meanwhile, the δ^{202}Hg signatures of anthropogenic emissions from regional

and long-range transport might be largely obscured by photo-reduction process, which well explains the positive δ^{202}Hg at the DMS. In contrast, the variation of Δ^{199}Hg at the CX was not associated with $Hg_{PM2.5}$ contents or δ^{202}Hg. The result suggests an insignificant impact of photo-reduction of Hg^{2+} relative to anthropogenic sources on the MDF and Hg content in $PM_{2.5}$ at the CX.

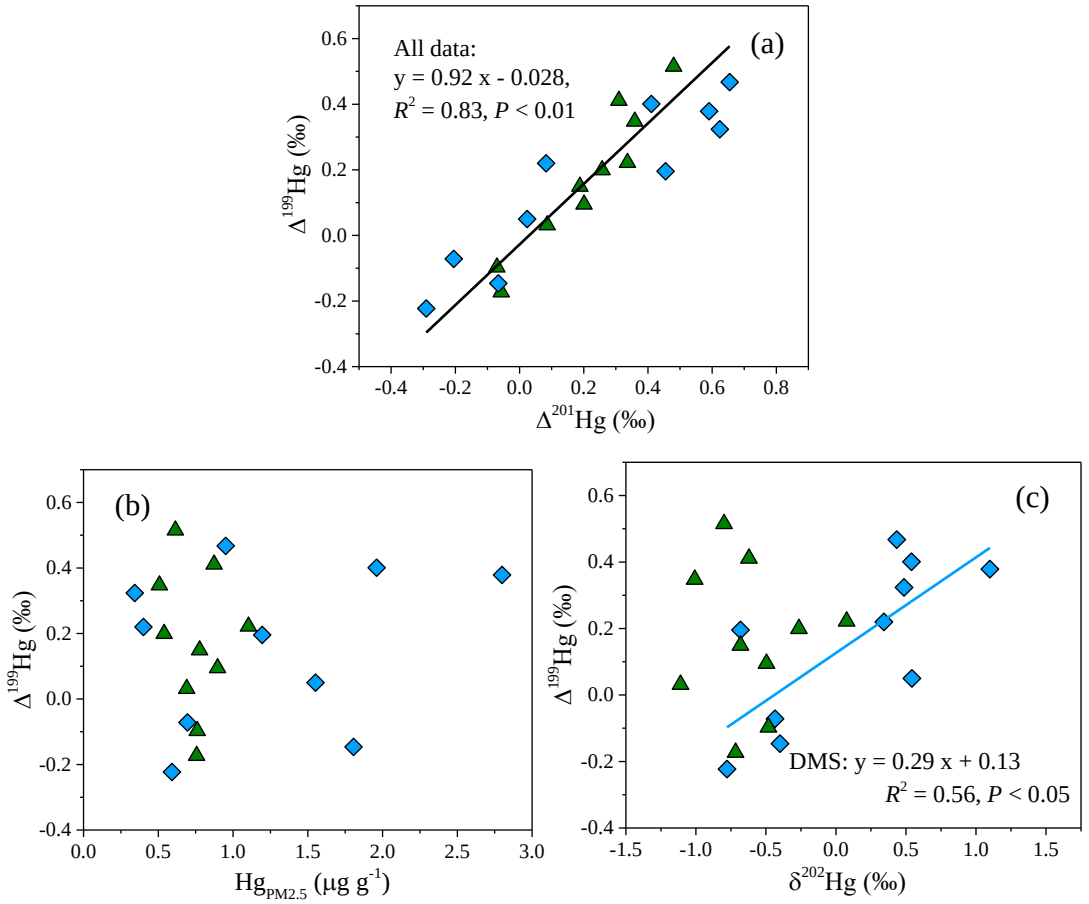

Fig. 4 Linear relationships between (a) Δ^{199}Hg and Δ^{201}Hg, (b) Δ^{199}Hg and $Hg_{PM2.5}$ content, and (c) Δ^{199}Hg and δ^{202}Hg at the CX (▲) and DMS (◆). Uncertainty (2σ) for Δ^{199}Hg and δ^{202}Hg in $PM_{2.5}$ is 0.03‰ and 0.25‰, respectively.

3.4. Potential mechanism of even-MIF

A small but significant MIF of ^{200}Hg was observed in most $PM_{2.5}$ samples from this study, with mean Δ^{200}Hg values of 0.11 ± 0.07‰ at the CX and 0.14 ± 0.07‰ at the DMS. They are more positive than those in urban (mean = 0.01‰ to 0.09‰, Das et al., 2016; Huang et al., 2016; Xu et al., 2017) and remote areas (mean = 0.07‰ to 0.10‰, Fu et al., 2019), but similar to those in coastal areas and island (Fu et al., 2019; Rolison et al., 2013). In general, Hg emitted from anthropogenic sources has Δ^{200}Hg of near-zero (Sun et al., 2016b), while large Δ^{200}Hg values are mainly observed in

atmospheric samples, i.e., precipitation, gaseous Hg^{2+}, and aerosols (Chen et al., 2012; Fu et al., 2019; Rolison et al., 2013). Significant even-MIF of Hg isotopes has been suggested to associate with photo-oxidation of Hg^0, from upper troposphere or/and from in situ involving UV light and oxidants (Chen et al., 2012; Fu et al., 2019). This could help explain significant $\Delta^{200}Hg$ values in coastal areas where halogen atoms are expected to be abundant. The $\Delta^{200}Hg$ values in $PM_{2.5}$ were not different between sites, similar to $\Delta^{199}Hg$ values, which supports that the observed $\Delta^{200}Hg$ were associated with photo-chemical processes of minor spatial difference.

Gaseous elemental Hg is the predominant form of Hg in atmosphere, which in China was generally characterized by slight negative even-MIF and odd-MIF (Fu et al., 2018; Yu et al., 2020). Given that gas-particle partitioning of Hg^{2+} is strongly temperature-dependent, this process unlikely produces the MIF of Hg isotopes (Fu et al., 2019). Thus, comparing the MIF of Hg isotopes between Hg^0 and Hg_{PM} might shed light on the effect of species conversion on Hg isotopes. The experimental study showed that the oxidation of Hg^0 vapor by Cl· or Br· results in positive $\Delta^{200}Hg$ values in products (Sun et al., 2016a). Thus, this process, which generally enhances in the coastal environment with abundant halogen atoms (Wang et al., 2019), would well explain for the detectable positive $\Delta^{200}Hg$ values in products. However, the oxidation of Hg^0 by Cl· or Br· should produce a negative odd-MIF in products (Sun et al., 2016a), which is inconsistent with the observed positive $\Delta^{199}Hg$ in $PM_{2.5}$. A recent study has reported that oxidation of Hg^0 by oxidizers other than Cl· or Br· might induce a positive odd-MIF in the Hg^{2+}, but this deduction lied on limit isotopic study of Hg^0 oxidation (Yu et al., 2020). Alternatively, the magnitude of photo-reduction of Hg^{2+} larger than the oxidation of Hg^0 by Cl and Br atoms could result in the observed positive odd-MIF of Hg_{PM}. Since photo-reduction of Hg^{2+} most likely occurred in aerosols as previously discussed, oxidation of Hg^0 and consequent photo-reduction of Hg^{2+} in aerosols was the possible cause of the positive $\Delta^{199}Hg$ and $\Delta^{200}Hg$ values of $PM_{2.5}$ in the study region.

3.5. Isotopes of Hg in adjacent surface seawater

Hg isotopes are often used to track the transport and transformations of Hg in the

environment. The average concentration of THg in seawater was 10.5 ± 5.0 ng L^{-1}, with a range of 1.9 ~ 23.6 ng L^{-1} (Table S1). As shown in Fig. 5, the concentrations of seawater THg displayed distinct time variations, with higher levels during Sep. ~ Mar. than during Apr. ~ Aug, which is likely related to the precipitation cycle. The average δ^{202}Hg value of seawater samples was -1.31 ± 0.59‰, with most samples fell in the range of -2.00‰ ~ -1.00‰. Whereas the MIF of Hg isotopes in seawater samples was not significant, with mean Δ^{199}Hg, Δ^{201}Hg, and Δ^{200}Hg values of -0.02 ± 0.07‰, 0.00 ± 0.05‰, and 0.04 ± 0.03‰, respectively. The negative MDF and near-zero MIF of surface seawater are well consistent with those of source materials (Huang et al., 2016; Sun et al., 2016b), suggesting the dominant effect of anthropogenic emissions on Hg in offshore surface seawater. A minor change in the intensity of industrial activities as expected among the months also supports the above deduction.

Isotopic compositions of THg in surface seawater and Hg_{PM} at the adjacent industrial site are consistent in MDF but not in MIF. Similar results were obtained comparing to wet deposition which presented negative δ^{202}Hg and positive Δ^{199}Hg and Δ^{200}Hg values (Chen et al., 2012; Huang et al., 2018). The negative MDF of Hg in industrial $PM_{2.5}$ and adjacent surface seawater implies an important contribution of local anthropogenic sources. On the other hand, the unity slope of Δ^{199}Hg versus Δ^{201}Hg ($\Delta^{199}Hg = 1.12 \times \Delta^{201}Hg - 0.02$, $R^2 = 0.68$, n = 19, Fig. S3) indicates that the odd-MIF of Hg isotopes in surface seawater was mainly produced by photo-reduction of Hg^{2+}. Whereas, the minor Δ^{199}Hg anomalies suggest that photo-reduction was not evident for surface seawater. A big discrepancy in the MIF of Hg isotopes between atmospheric samples and surface seawater further evidences that atmospheric transformations would induce the significant MIF of Hg isotopes and obscure the Hg isotopic signatures of anthropogenic emissions.

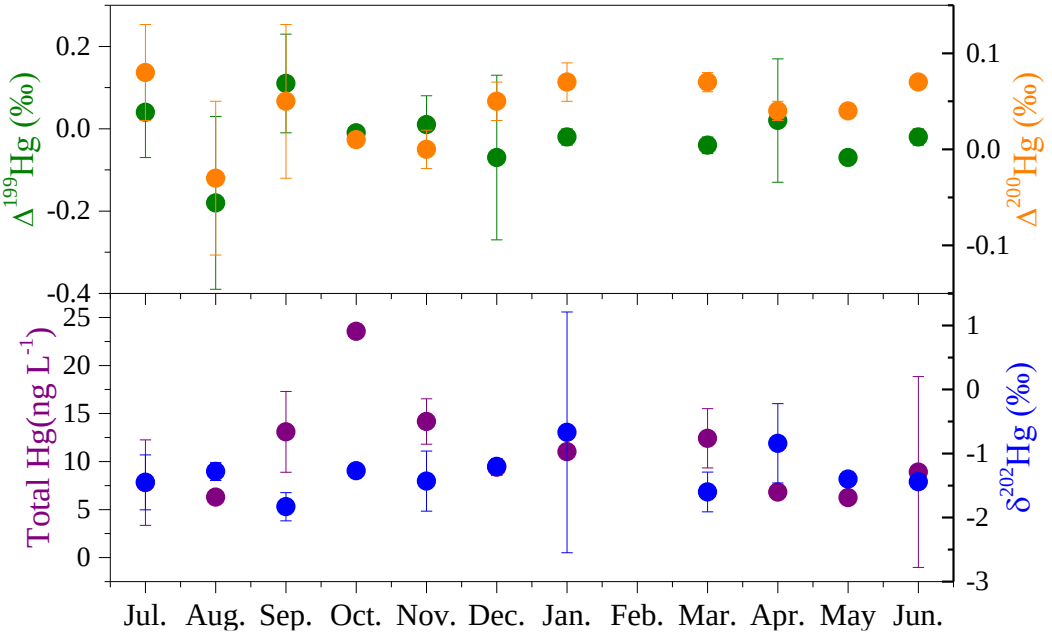

Fig. 5 Monthly variations of total Hg concentration, δ^{202}Hg, Δ^{199}Hg and Δ^{200}Hg of surface seawater during the sampling period from July 2017 to June 2018

4. Conclusion

This study investigated Hg isotopic compositions in $PM_{2.5}$ collected from the neighboring industrial and mountain sites in a coastal area and in surface seawater close to the industrial area. $Hg_{PM2.5}$ displayed a significant spatial difference in MDF but not in odd-MIF. Negative δ^{202}Hg in $PM_{2.5}$ at the CX was primarily induced by local industrial activities like coal combustion. Whereas, the slight positive δ^{202}Hg at the DMS could not be fully explained by anthropogenic emissions. Other than the effect of regional transport, a close correlation between δ^{202}Hg and Δ^{199}Hg at the DMS implies that photo-chemical processes likely contributed to the MDF of $Hg_{PM2.5}$. Significant positive odd-MIF of $Hg_{PM2.5}$ and the unity slope of Δ^{199}Hg versus Δ^{201}Hg indicate an important role of photo-reduction of Hg^{2+} in aerosols. The observed positive Δ^{200}Hg values in this study were probably associated with photo-oxidation of Hg^0 which is generally enhanced in the coastal environment. THg in surface seawater was characterized by negative MDF and near-zero odd-MIF, which is more consistent with isotopic signatures of source materials. The MIF anomalies of Hg isotopes were larger for atmospheric $PM_{2.5}$ than for surface seawater, suggesting that atmospheric transformations induce significant MIF of Hg isotopes and obscure Hg isotopic signatures of initial anthropogenic emissions.

Novelty statement

A comparison of isotopic compositions of $Hg_{PM2.5}$ was conducted between the neighboring industrial and mountain sites, which effectively revealed the influence of anthropogenic emission sources and transformation processes on Hg isotopes. Hg isotopic compositions in industrial $PM_{2.5}$ and ~~in~~ offshore surface seawater were also compared. The results indicate that atmospheric transformations would induce significant fractionation of Hg isotopes and obscure specific Hg isotopic signatures of initial emissions.~~–~~

Data availability. HYSPLIT trajectory model and gridded meteorological data (Global Data Assimilation System, GDAS1) are available from the US National Oceanic and Atmospheric Administration (http://ready.arl.noaa.gov). Fire data are available in the Fire Information for Resource Management System (FIRMS, https://firms2.modaps.eosdis.nasa.gov/map/#d:2021-04-26..2021-04-27;@6.7,2.0,3z). All data in this study are available upon request to the first author via email (linglingxu@iue.ac.cn).

Author contributions. JSC, LLX, and YRZ designed this study. MRL, LQY, YTC, LT and HX conducted the sampling. YRZ and LLX participated in sample treatment and measurements. LLX wrote the paper. JYS and YPC helped the graphics production. All authors reviewed the paper.

Competing interests. The authors declare that they have no conflict of interest.

Acknowledgements. This research was financially supported by National Natural Science Foundation of China (No. 21507127; 41575146 & U1405235), Natural Science Foundation of Fujian province (2016J05050), the Cultivating Project of Strategic Priority Research Program of Chinese Academy of Sciences (XDPB1903), the CAS Center for Excellence in Regional Atmospheric Environment (E0L1B20201), and Xiamen Atmospheric Environment Observation and Research Station of Fujian

Province. We would like to thank Shuyuan Huang (Xiamen University) for his help in Hg isotopes analysis. We also thank the handling editor and two reviewers for their constructive comments and suggestions.

References

Bergquist, B. A. and Blum, J. D.: Mass-dependent and -independent fractionation of Hg isotopes by photoreduction in aquatic systems, Science, 318, 417–420, doi: 10.1126/science.1148050, 2007.

Biswas, A., Blum, J. D., Bergquist, B. A., Keeler, G. J., Xie, Z. Q.: Natural mercury isotope variation in coal deposits and organic soils, Environ. Sci. Technol., 42(22), 8303−8309, doi: 10.1021/es801444b, 2008.

Blum, J. D. and Bergquist, R. A.: Reporting of variations in the natural isotopic composition of mercury, Anal. Bioanal. Chem., 338(2), 353–359, doi: org/10.1007/s00216-007-1236-9, 2007.

Blum, J. D., Sherman, L. S., Johnson, M. W.: Mercury isotopes in earth and environmental sciences, Annu. Rev. Earth Planet. Sci., 42, 249–269, doi: 10.1146/annurev-earth-050212-124107, 2014.

Blum, J. D. and Johnson, M. W.: Recent developments in mercury stable isotope analysis, Non-Traditional Stable Isotopes, 82, 733-757, doi: 10.2138/rmg.2017.82.17, 2017.

Chen, J. B., Hintelmann, H., Feng, X. B., Dimock, B.: Unusual fractionation of both odd and even mercury isotopes in precipitation from Peterborough, ON, Canada, Geochim. Cosmochim. Ac., 90, 33−46, doi: 10.1016/j.gca.2012.05.005, 2012.

Das, R., Wang, X. F., Khezri, B., Webster, R. D., Sikdar, P. K., Datta, S.: Mercury isotopes of atmospheric particle bound mercury for source apportionment study in urban Kolkata, India, Elementa-Sci. Anthrop., 4, 1−12, doi: 10.12952/journal.elementa.000098, 2016.

Demers, J. D., Blum, J. D., Zak, D. R.: Mercury isotopes in a forested ecosystem: Implications for air-surface exchange dynamics and the global mercury cycle, Global Biogeochem. Cy., 27(1), 222−238, doi: 10.1002/gbc.20021, 2013.

Fu, X. W., Zhang, H., Yu, B., Wang, X., Lin, C.-J., and Feng, X. B.: Observations of atmospheric mercury in China: a critical review, Atmos. Chem. Phys., 15, 9455–9476, doi:10.5194/acp-15-94552015, 2015.

Fu, X. W., Yang, X., Tan, Q. Y., Ming, L. L., Lin, T., Lin, C.-J., Li, X. D., Feng, X. B.: Isotopic composition of gaseous elemental mercury in the marine boundary layer of East China Sea, J. Geophys. Res.: Atmos., 123, 7656–7669, doi: 10.1029/2018JD028671, 2018.

Fu, X. W., Zhang, H., Feng, X. B., Tan, Q. Y., Ming, L. L., Liu, C., Zhang, L. M.: Domestic and transboundary sources of atmospheric particulate bound mercury in remote areas of China: Evidence from mercury isotopes, Environ. Sci. Technol., 53(4), 1947−1957, doi: 10.1021/acs.est.8b06736, 2019.

GMA: Global Mercury Assessment 2018. UN Environment Programme, Chemicals and Health Branch Geneva, Switzerland.

Guo, J. M., Sharma, C. M., Tripathee L., Kang, S. C., Fu, X. W., Huang, J., Shrestha K. L., Chen, P. F.: Source identification of atmospheric particle-bound mercury in the Himalayan foothills through non-isotopic and isotope analyses, Environ. Pollut., 286, 117317, doi: 10.1016/j.envpol.2021.117317, 2021.

Guo, J. M., Tripathee, L., Kang, S. C., Zhang, Q. G., Huang, J., Sharma, C. M., Chen, P. F., Paudyal, R., Rupakheti, D.: Atmospheric particle-bound mercury in the northern Indo-Gangetic Plain region: Insights into sources from mercury isotope analysis and influencing factors, Geosci. Front., 13, 101274, doi: 10.1016/j.gsf.2021.101274, 2022.

Horowitz, H. M., Jacob, D. J., Zhang, Y. X., Dibble, T. S., Slemr, F., Amos, H. M., Schmidt, J. A., Corbitt, E. S., Marais, E. A., Sunderland, E. M.: A new mechanism for atmospheric mercury redox chemistry: implications for the global mercury budget, Atmos. Chem. Phys., 17(10), 6353−6371, doi: org/10.5194/acp-17-6353-2017, 2017.

Hong, Y. W., Chen, J. S., Deng, J. J., Tong, L., Xu, L. L., Niu, Z. C., Yin, L. Q., Chen, Y. T., Hong, Z. Y.: Pattern of atmospheric mercury speciation during episodes of elevated PM2.5 levels in a coastal city in the Yangtze River Delta, China,

Environ. Pollut., 218, 259-268, doi: 10.1016/j.envpol.2016.06.073, 2016.

Hong, Z. Y., Zhang, H., Zhang, Y. R., Xu, L. L., Liu, T. T., Xiao, H., Hong, Y. W., Chen, J. S., Li, M. R., Deng, J. J., Wu, X., Hu, B. Y., Chen, X. Q.: Secondary organic aerosol of PM2.5 in a mountainous forest area in southeastern China: Molecular compositions and tracers implication, Sci, Total Environ. 653: 496−503, doi: 10.1016/j.scitotenv.2018.10.370, 2019.

Huang, Q., Liu, Y. L., Chen, J. B., Feng, X. B., Huang, W. L., Yuan, S. L., Cai, H. M., Fu, X. W.: An improved dual-stage protocol to pre-concentrate mercury from airborne particles for precise isotopic measurement, J. Anal. Atom. Spectrom., 30(4), 957−966, doi: 10.1039/c4ja00438h, 2015.

Huang, Q., Chen, J. B., Huang, W. L., Fu, P. Q., Guinot, B., Feng, X. B., Shang, L. H., Wang, Z. H., Wang, Z. W., Yuan, S. L., Cai, H. M., Wei, L. F., Yu, B.: Isotopic composition for source identification of mercury in atmospheric fine particles, Atmos. Chem. Phys., 16(18), 11773–11786, doi:10.5194/acp-16-11773-2016, 2016.

Huang, S. Y., Sun, L. M., Zhou, T. J., Yuan, D. X., Du, B., Sun, X. W.: Natural stable isotopic compositions of mercury in aerosols and wet precipitations around a coal-fired power plant in Xiamen, southeast China, Atmos. Environ., 173, 72−80, doi: 10.1016/j.atmosenv.2017.11.003, 2018.

Huang, Q., Chen, J. B., Huang, W. L., Reinfelder, J. R., Fu, P. Q., Yuan, S. L., Wang, Z. W., Yuan, W., Cai, H. M., Ren, H., Sun, Y. L., He, L.: Diel variation in mercury stable isotope ratios records photoreduction of PM2.5-bound mercury, Atmos. Chem. Phys., 19(1), 315−325, doi: 10.5194/acp-19-315-2019, 2019.

Huang, Q., Reinfelder, J. R., Fu, P. Q., Huang, W. L.: Variation in the mercury concentration and stable isotope composition of atmospheric total suspended particles in Beijing, China, J. Hazard. Mater., 383, 121131, doi: 10.1016/j.jhazmat. 2019.121131, 2020.

Huang, S. Y., Zhao, Y. H., Lv, S. P., Wang, W. G., Wang, W. L., Zhang, Y. B., Huo, Y. L., Sun, X. W., Chen, Y. J.: Distribution of mercury isotope signatures in Yundang Lagoon, Xiamen, China, after long-term interventions, Chemosphere,

688 272, 129716, doi: 10.1016/j.chemosphere.2021.129716, 2021.
689 Jiskra, M., Wiederhold, J. G., Skyllberg, U., Kronberg, R. M., Hajdas, I., Kretzschmar,
690 R.: Mercury deposition and re-emission pathways in boreal forest soils
691 investigated with Hg isotope signatures, Environ. Sci. Technol., 49(12),
692 7188−7196, doi: 10.1021/acs.est.5b00742, 2015.
693 Lin, H. Y., Yuan, D. X., Lu, B. Y., Huang, S. Y., Sun, L. M., Zhang, F., Gao, Y. Q.:
694 Isotopic composition analysis of dissolved mercury in seawater with purge and
695 trap preconcentration and a modified Hg introduction device for MC-ICP-MS, J.
696 Anal. Atom. Spectrom., 30(2), 353−359, doi: 10.1039/c4ja00242c, 2015.
697 Malinovsky, D., Latruwe, K., Moens, L., Vanhaecke, F.: Experimental study of
698 mass-independence of Hg isotope fractionation during photodecomposition of
699 dissolved methylmercury, J. Anal. Atom. Spectrom., 25(7), 950-956, doi:
700 10.1039/b926650j, 2010.
701 Mao, H. T., Cheng, I., Zhang, L. M.: Current understanding of the driving
702 mechanisms for spatiotemporal variations of atmospheric speciated mercury: a
703 review, Atmos. Chem. Phys., 16(20), 12897-12924, doi:
704 10.5194/acp-16-12897-2016, 2016.
705 Rolison, J. M., Landing, W. M., Luke, W., Cohen, M., Salters, V. J. M.: Isotopic
706 composition of species-specific atmospheric Hg in a coastal environment, Chem.
707 Geol., 336, 37−49, doi: 10.1016/j.chemgeo.2012.10.007, 2013.
708 Schroeder, W. H. and Munthe J.: Atmospheric mercury—An overview, Atmos.
709 Environ., 32(5), 809–822, doi:10.1016/S1352-2310(97) 00293-8, 1998.
710 Schleicher, N. J., Schäfer, J., Blanc, G., Chen, Y., Chai, F., Cen, K., Norra, S.:
711 Atmospheric particulate mercury in the megacity Beijing: spatio-temporal
712 variations and source apportionment, Atmos. Environ., 109, 251–261, doi:
713 10.1016/j.atmosenv.2015.03.018, 2015.
714 Selin, N. E.: Global biogeochemical cycling of mercury: A review, Annu. Rev. Env.
715 Resour., 34, 43–63, doi: 10.1146/annurev.environ.051308.084314, 2009.
716 Sonke, J. E. and Blum, J. D.: Advances in mercury stable isotope biogeochemistry
717 preface, Chem. Geol., 336, 1–4, doi: 10.1016/j.chemgeo.2012.10.035, 2013.

718 Sun, R. Y., Heimburger, L. E., Sonke, J. E., Liu, G. J.: Mercury stable isotope
719 fractionation in six utility boilers of two large coal-fired power plants, Chem.
720 Geol., 336, 103−111, doi: 10.1016/j.chemgeo.2012.10.055, 2013.
721 Sun, R. Y., Sonke, J. E., Heimburger, L. E., Belkin, H. E., Liu, G. J., Shome, D.,
722 Cukrowska, E., Liousse, C., Pokrovsky, O. S., Streets, D. G.: Mercury stable
723 isotope signatures of world coal deposits and historical coal combustion
724 emissions, Environ. Sci. Technol., 48(13), 7660−7668, doi: 10.1021/es501208a,
725 2014.
726 Sun, G. Y., Sommar, J., Feng, X. B., Lin, C.-J., Ge, M. F., Wang, W. G., Yin, R. S., Fu,
727 X. W., Shang, L. H.: Mass-dependent and -independent fractionation of mercury
728 isotope during gas-phase oxidation of elemental mercury vapor by atomic Cl and
729 Br, Environ. Sci. Telchnol., 50(17), 9232−9241, doi: 10.1021/acs.est.6b01668,
730 2016a.
731 Sun, R. Y., Streets, D. G., Horowitz, H. M., Amos, H. M., Liu, G. J., Perrot, V., Toutain,
732 J.P., Hintelmann, H., Sunderland, E. M., Sonke, J. E.: Historical (1850-2010)
733 mercury stable isotope inventory from anthropogenic sources to the atmosphere,
734 Elementa-Sci. Anthrop., 4, 1−15, doi: 10.12952/journal.elementa.000091, 2016b.
735 Wang, S. Y., McNamara, S. M., Moore, C. W., Obrist, D., Steffen, A., Shepson, P. B.,
736 Steabler, R. M., Raso, A. R. W., Pratt, K. A.: Direct detection of atmospheric
737 atomic bromine leading to mercury and ozone depletion, P. Natl. Acad. Sci.,
738 116(29), 14479−14484, doi: 10.1073/pnas.1900613116, 2019.
739 Wiederhold, J. G.; Cramer, C. J.; Daniel, K.; Infante, I.; Bourdon, B.; Kretzschmar, R.:
740 Equilibrium mercury isotope fractionation between dissolved Hg(II) species and
741 thiol-bound Hg, Environ. Sci. Technol., 44 (11), 4191−4197, doi:
742 10.1021/es100205t, 2010.
743 Xu, L. L., Chen, J. S., Yang, L. M., Yin, L. Q., Yu, J. S., Qiu, T. X., Hong, Y.W.:
744 Characteristics of total and methyl mercury in wet deposition in a coastal city,
745 Xiamen, China: Concentrations, fluxes and influencing factors on Hg
746 distribution in precipitation, Atmos. Environ. 99, 10−16, doi:
747 10.1016/j.atmosenv.2014.09.054, 2014.

748 Xu, H. M., Sonke, J. E., Guinot, B., Fu, X. W., Sun, R. Y., Lanzanova, A., Candaudap,
749 F., Shen, Z. X., Cao, J. J.: Seasonal and annual variations in atmospheric Hg and
750 Pb isotopes in Xi'an, China, Environ. Sci. Technol., 51(7), 3759−3766, doi:
751 10.1021/acs.est.6b06145, 2017.
752 Xu, L. L., Jiao, L., Hong, Z. Y., Zhang, Y. R., Du, W. J., Wu, X., Chen, Y. T., Deng, J.
753 J., Hong, Y. W., Chen, J. S.: Source identification of $PM_{2.5}$ at a port and an
754 adjacent urban site in a coastal city of China: Impact of ship emissions and port
755 activities, Sci. Total Environ., 634: 1205 − 1213, doi:
756 10.1016/j.scitotenv.2018.04.087, 2018.
757 Xu, H. M., Sun, R. Y., Cao, J. J., Huang, R. J., Guinot, B., Shen, Z. X., Jiskra, M., Li,
758 C. X., Du, B. Y., He, C., Liu, S.X., Zhang, T., Sonke, J. E.: Mercury stable
759 isotope compositions of Chinese urban fine particulates in winter haze days:
760 Implications for Hg sources and transformations, Chem. Geol., 504, 267−275,
761 doi: 10.1016/j.chemgeo.2018.11.018, 2019.
762 Xu, L. L., Zhang, Y. R., Tong, L., Chen, Y. P., Zhao, G. Q., Hong, Y. W., Xiao, H.,
763 Chen, J. S.: Gas-particle partitioning of atmospheric reactive mercury and its
764 contribution to particle bound mercury in a coastal city of the Yangtze River
765 Delta, China, Atmos. Environ., 239, 117744, doi:
766 10.1016/j.atmosenv.2020.117744, 2020.
767 Yin, R. S., Feng, X. B., Meng, B.: Stable mercury isotope variation in rice plants
768 (Oryza sativa L.) from the Wanshan mercury mining district, SW China, Environ.
769 Sci. Technol., 47(5), 2238−2245, doi: 10.1021/es304302a, 2013.
770 Yin, R. S., Feng, X. B., Li, X. D., Yu, B., Du, B. Y.: Trends and advances in mercury
771 stable isotopes as a geochemical tracer, Trends Environ. Anal., 2, 1−10, doi:
772 10.1021/es500322n, 2014a.
773 Yin, R. S., Feng, X. B., Chen, J. B.: Mercury stable isotopic compositions in coals
774 from major coal producing fields in China and their geochemical and
775 environmental Implications, Environ. Sci. Technol., 48(10), 5565−5574, doi:
776 10.1021/es500322n, 2014b.

Yin, R. S., Feng, X. B., Hurley, J. P., Krabbenhoft, D. P., Lepak, R. F., Hu, R. Z., Zhang, Q., Li, Z. G., Bi, X. W.: Mercury isotopes as proxies to identify sources and environmental impacts of mercury in Sphalerites, Sci. Rep., 6, 2045−2322, doi: 10.1038/srep18686, 2016.

Yu, B., Wang, X., Lin, C. J., Fu, X. W., Zhang, H., Shang, L. H., Feng, X. B.: Characteristics and potential sources of atmospheric mercury at a subtropical near-coastal site in East China, J. Geophys. Res.-Atmospheres, 120(16), 8563−8574, doi:10.1002/2015JD023425, 2015.

Yu, B., Fu, X. W., Yin, R. S., Zhang, H., Wang, X., Lin, C. J., Wu, C. S., Zhang, Y. P., He, N. N., Fu, P. Q., Wang, Z. F., Shang, L. H., Sommar, J., Sonke, J. E., Maurice, L., Guinot, B., Feng, X. B.: Isotopic composition of atmospheric mercury in China: New evidence for sources and transformation processes in air and in vegetation, Environ. Sci. Technol., 50(17), 9262−9269, doi: 10.1021/acs.est.6b01782, 2016.

Yu, B., Yang, L., Wang, L. L., Liu, H. W., Xiao, C. L., Ling, Y., Liu, Q., Yin, Y. G., Hu, L. G., Shi, J. B., Jiang, G. B.: New evidence for atmospheric mercury transformations in the marine boundary layer from stable mercury isotopes, Atmos. Chem. Phys., 20, 9713−9723, doi: 10.5194/acp-20-9713-2020, 2020.

Zhang, L., Wang, S. X., Wang, L., Wu, L., Duan, L., Wu, Q. R., Wang, F. Y., Yang, M., Yang, H., Hao, J. M., Liu, X.: Updated emission inventories for speciated atmospheric mercury from anthropogenic sources in China, Environ. Sci. Technol., 49(5), 3185−3194, doi: 10.1021/es504840m, 2015.

Zheng, W. and Hintelmann, H.: Mercury isotope fractionation during photoreduction in natural water is controlled by its Hg /DOC ratio, Geochim. Cosmochim. Ac., 73, 6704–6715, doi: 10.1016/j.gca.2009.08.016, 2009.

Zheng, W., Obrist, D., Weis, D., Bergquist, B. A.: Mercury isotope compositions across North American forests, Global Biogeochem. Cy., 30(10), 1475−1492, doi: 10.1002/2015gb005323, 2016.